Available online at www.sciencedirect.com

ScienceDirect

Journal of the European Ceramic Society 31 (2011) 3137–3143

www.elsevier.com/locate/jeurceramsoc

The effects of doped Nd on conductivity and phase stability of $BaCe_{0.8}Y_{0.2}O_{3-\delta}$-based electrolyte for solid oxide fuel cell

Yu-Chen Lee *, I-Ming Hung, Shu-Luen Chang, Chun-Jing Ciou, Jun-Sheng Wu

Yuan Ze Fuel Cell Center/Department of Chemical Engineering and Materials Science, Yuan Ze University, No. 135, Yuan-Tung Road, Chungli, Taoyuan 320, Taiwan

Available online 31 May 2011

Abstract

This study investigates the structure, phase stability, and electrical properties of $BaCe_{0.8}Y_{0.2-x}Nd_xO_{3-\delta}$ (x = 0–0.2) in humid air. XRD results indicate that a $BaCe_{0.8}Y_{0.2-x}Nd_xO_{3-\delta}$ sample has an asymmetric orthorhombic structure, and this structure becomes more symmetric as the amount of Nd doping increases. The conductivity of $BaCe_{0.8}Y_{0.2-x}Nd_xO_{3-\delta}$ depends on the amount of Nd doping and the operation temperature. AC impedance results indicate that the resistance of $BaCe_{0.8}Y_{0.2-x}Nd_xO_{3-\delta}$ decreases as the temperature increases, with the majority of resistance coming from oxygen ion diffusion. The XRD peak intensity of $BaCe_{0.8}Y_{0.2}O_{3-\delta}$ apparently decreased with time, forming $Ba(OH)_2$ and CeO_2 second phases. The phase stability of $BaCe_{0.8}Y_{0.2-x}Nd_xO_{3-\delta}$ (x = 0.05–0.2) samples is much better than that of $BaCe_{0.8}Y_{0.2}O_{3-\delta}$, and it exhibited no second phase after tested in an 80 °C water bath for 18 h.

Keywords: Powders-solid state reaction; Ionic conductivity; Perovskites; Fuel cells; Impedance

1. Introduction

Solid oxide fuel cells (SOFCs) are highly efficient and clean electrochemical power-generation systems because of their high energy conversion efficiency, high power density, environmental friendliness, and flexibility in using fuels.[1] A conventional high-temperature SOFC (HT-SOFC) based on a 8 mol% yttria-stabilized zirconia (YSZ) electrolyte operates at a high temperature range of 800–1000 °C. However, this high operation temperature causes many problems such as high cost, special materials for sealing and the current interconnector, chemical reactions, and thermal expansion mismatch between the components, and a long start-up/shut-off period. Lowering the operation temperature of SOFCs to 600–800 °C using high-conductivity electrolyte materials[2–5] widens the choice of possible metal interconnectors, significantly reduces production and application costs, and improves overall SOFC stability and reliability.

Cation-doped $BaCeO_3$ attracted great interest in the 1980s and 1990s due to their high ionic conductivity at 400–700 °C. Iwahara et al. demonstrated that $BaCeO_3$ has the highest conductivity among the high temperature proton conductors (HTPCs).[6] Researchers recently demonstrated a SOFC based on $BaCe_{0.8}Y_{0.2}O_3$ electrolyte with a power density of 0.9 and 1.4 W cm^{-2} at operating temperatures of 400 °C and 600 °C, respectively.[7–10] However, this cation-doped $BaCeO_3$ electrolyte has not yet been commercialized because it has a phase stability problem under SOFC operation conditions, such as humid air and an atmosphere containing CO_2.[11] Therefore, it is necessary to ensure that the electrolyte materials have thermodynamic stability or at least long-term kinetic stability with good conductivity. Previous research indicates that phase stability is a serious concern for $BaCeO_3$-based electrolytes. Recent studies demonstrate the many effects of adjusting the chemical composition of the $BaCeO_3$-based ionic conductor or coating it with a protective layer to prevent degradation.[5,12]

This study investigates the structure and conductivity of $BaCe_{0.8}Y_{0.2-x}Nd_xO_{3-\delta}$ (x = 0–0.2) in humid air in detail. This is also the first study to show that the phase stability and decomposition thermodynamics of $BaCe_{0.8}Y_{0.2-x}Nd_xO_{3-\delta}$ (x = 0–0.2) depend on time in 80 °C water.

2. Experimental

$BaCe_{0.8}Y_{0.2-x}Nd_xO_{3-\delta}$ (x = 0–0.2) powders were prepared through a solid-state reaction process. The stoichiometric ratios

* Corresponding author. Tel.: +886 3 4638800x2569; fax: +886 3 4630634.
E-mail address: s998806@mail.yzu.edu.tw (Y.-C. Lee).

0955-2219/$ – see front matter © 2011 Elsevier Ltd. All rights reserved.
doi:10.1016/j.jeurceramsoc.2011.05.003

of high purity oxide powders of $BaCO_3$ (J.T. Baker, 99.9%), CeO_2 (Alfa, 99.9%), Y_2O_3 (Alfa, 99.99%) and Nd_2O_3 (Alfa, 99.99%) were mixed and ball milled in ethanol for 24 h. The dried powders were subsequently calcined at 1300 °C in air for 12 h. The calcined powder is die-pressed into pellets measuring approximately 1 cm diameter and 2 mm thick under 25 kg/cm^2 of pressure. Finally, the samples sintered at 1600 °C for 4 h in air.

Thermogravimetry analysis (TGA) was performed from 30 °C to 1000 °C at a heating rate of 5 °C/min in air using TA Instruments SDT-Q600 DSC-TGA. The phase identification of the $BaCe_{0.8}Y_{0.2-x}Nd_xO_{3-\delta}$ powders were performed with a powder diffractometer (LabX, XRD-6000) with Ni-filtered Cu Kα radiation and a diffraction angle ranging from 20° to 85° with a step of 0.01° and a rate of 1°/min. The conductivity of samples was measured in 3 RH% humid air in a temperature range of 450–750 °C using a DC two-probe method and Agilent 34970a. The conductivity was calculated according to Eq. (1) as follows:

$$\sigma = \frac{L}{A \times \Omega} \tag{1}$$

where σ is conductivity (S/cm), L is sample thickness (cm), A is sample area (cm^2), and Ω is electrical resistance (ohm).

The activation energy of conductivity was calculated using the Arrhenius equation as follows:

$$\sigma T = A e^{-E_a/RT} \tag{2}$$

where T is temperature (K), E_a is activation energy (J/mol), R is the gas constant (J/mol K), and A is pre-exponential constant.

The phase decomposition thermodynamics of $BaCe_{0.8}Y_{0.2-x}Nd_xO_{3-\delta}$ (x = 0–0.2) were calculated using the Fraction Life Method (t_F)[13] based on the XRD patterns in 80 °C water after 0, 6, 12, 18, and 24 h, respectively. The electrochemical impedance spectra (EIS) were measured using an impedance analyzer (HIOKI, 3522-50 and 3532-50) at 100 mV, from 50 kHz to 0.01 Hz frequency in humid air at temperatures ranging from 600 to 800 °C.

3. Results and discussion

Fig. 1 shows the XRD patterns of $BaCe_{0.8}Y_{0.2-x}Nd_xO_{3-\delta}$ calcined at 1300 °C for 12 h. The XRD pattern of $BaCe_{0.8}Y_{0.2}O_{3-\delta}$ main phase exhibits sub-peak patterns, indicating that the structure is a perovskite orthorhombic structure. Fig. 1A (b)–(e) shows the XRD patterns of $BaCe_{0.8}Y_{0.2-x}Nd_xO_{3-\delta}$ (x = 0.05–0.2), indicating that the structure is pseudo-orthorhombic structure. The peaks include the (1 1 0), (1 1 1), (2 0 0), (2 1 1), (2 2 0), (3 1 0), (2 2 2), and (3 2 1) reflections. Fig. 1B shows the XRD patterns of samples from 50° to 51.5°. The XRD patterns of depict the structure of apparently closer to orthorhombic structure. Table 1 lists the lattice parameters and unit volume of $BaCe_{0.8}Y_{0.2-x}Nd_xO_{3-\delta}$. These results indicate that the $BaCe_{0.8}Y_{0.2-x}Nd_xO_{3-\delta}$ structure changes to a more symmetric structure with Nd doping.

Fig. 2 shows the thermal gravity analysis (TGA) curves of $BaCe_{0.8}Y_{0.2-x}Nd_xO_{3-\delta}$ in air from room temperature to 1000 °C. This figure shows the weight of all $BaCe_{0.8}Y_{0.2-x}Nd_xO_{3-\delta}$ samples decreased as the temperature increased due to the oxygen loss, which in turn led to the formation of oxygen vacancies. A comparison with the mass loss curves of $BaCe_{0.8}Y_{0.2}O_{3-\delta}$ and $BaCe_{0.8}Y_{0.2-x}Nd_xO_{3-\delta}$ (x = 0.05–0.2) samples reveals that the weight of $BaCe_{0.8}Y_{0.2}O_{3-\delta}$ slightly increased above 800 °C, which may be due to the reaction of $BaCe_{0.8}Y_{0.2}O_{3-\delta}$ with CO_2 in air. However, the mass loss curve of $BaCe_{0.8}Y_{0.2-x}Nd_xO_{3-\delta}$

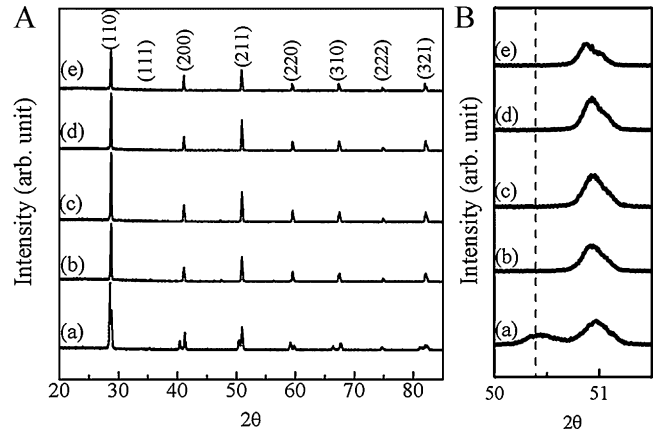

Fig. 1. (A) XRD patterns of (a) $BaCe_{0.8}Y_{0.2}O_{3-\delta}$; (b) $BaCe_{0.8}Y_{0.15}Nd_{0.05}O_{3-\delta}$; (c) $BaCe_{0.8}Y_{0.1}Nd_{0.1}O_{3-\delta}$; (d) $BaCe_{0.8}Y_{0.05}Nd_{0.15}O_{3-\delta}$; (e) $BaCe_{0.8}Nd_{0.2}O_{3-\delta}$ and (B) magnified XRD patterns from 50° to 51.5°.

Table 1
Lattice parameters and unit volume of $BaCe_{0.8}Y_{0.2-x}Nd_xO_{3-\delta}$.

Samples	a (Å)	b (Å)	c (Å)	V (Å^3)
$BaCe_{0.8}Y_{0.2}O_{3-\delta}$	8.7432	6.2750	6.2033	340.3380
$BaCe_{0.8}Y_{0.15}Nd_{0.05}O_{3-\delta}$	8.7570	6.2273	6.1930	337.7156
$BaCe_{0.8}Y_{0.1}Nd_{0.1}O_{3-\delta}$	8.7487	6.2279	6.1907	337.3071
$BaCe_{0.8}Y_{0.05}Nd_{0.15}O_{3-\delta}$	8.7576	6.2242	6.1914	337.4855
$BaCe_{0.8}Nd_{0.2}O_{3-\delta}$	8.7737	6.2235	6.2102	339.0951

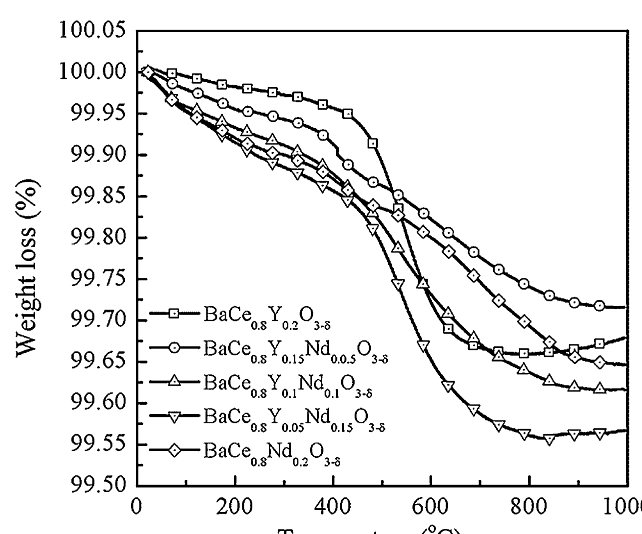

Fig. 2. Thermalgravity analysis curves of $BaCe_{0.8}Y_{0.2-x}Nd_xO_{3-\delta}$ in air with a heating rate of 5 °C/min.

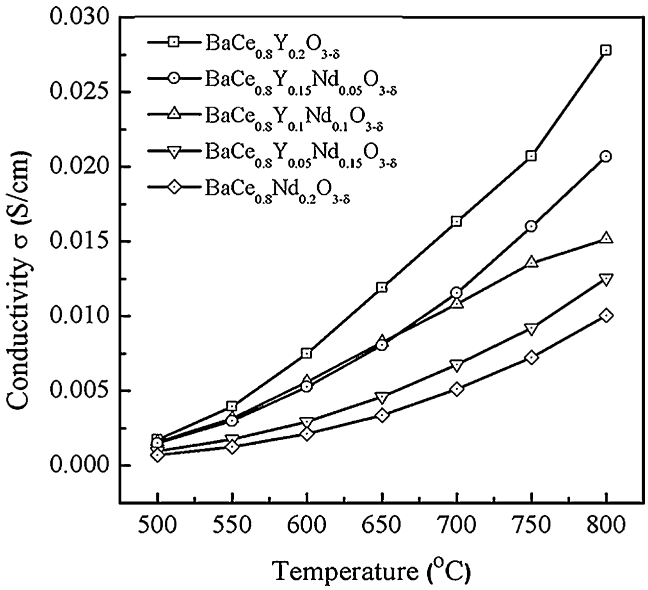

Fig. 3. Conductivity of $BaCe_{0.8}Y_{0.2-x}Nd_xO_{3-\delta}$ at different temperatures in 3 RH% air.

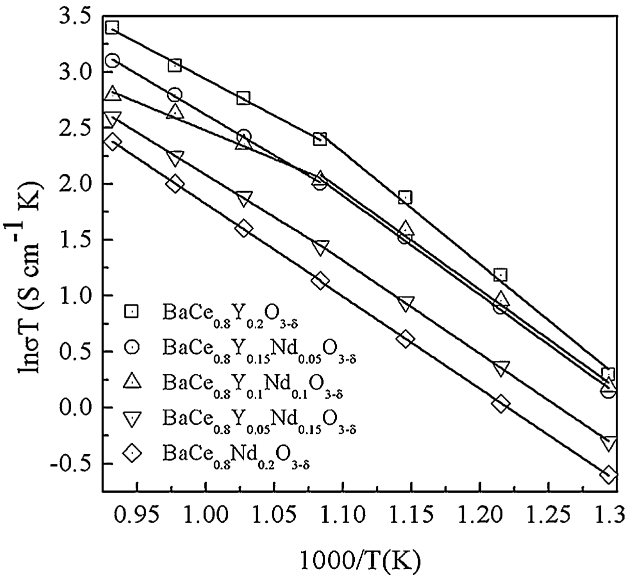

Fig. 4. Arrhenius plot of conductivity of $BaCe_{0.8}Y_{0.2-x}Nd_xO_{3-\delta}$ at different temperatures in 3 RH% air.

remained constant. This indicates that the phase stability of $BaCe_{0.8}Y_{0.2-x}Nd_xO_{3-\delta}$ is better than that of $BaCe_{0.8}Y_{0.2}O_{3-\delta}$.

Fig. 3 shows the conductivity of $BaCe_{0.8}Y_{0.2-x}Nd_xO_{3-\delta}$ samples as a function of temperature in air. The conductivity of all samples increased as the temperature increased. This indicates that the $BaCe_{0.8}Y_{0.2-x}Nd_xO_{3-\delta}$ is an ionic conductor. The conductivity of $BaCe_{0.8}Y_{0.2-x}Nd_xO_{3-\delta}$ decreased as the amount of Nd doping increased. The conductivity of $BaCe_{0.8}Y_{0.2}O_{3-\delta}$ decreased from 0.028 S/cm to 0.01 S/cm as the Nd doping increased from 0 to 20 mol%. The $BaCe_{0.8}Y_{0.1}Nd_{0.1}O_{3-\delta}$ exhibited the conductivity of 0.015 S/cm at 800 °C, which is much higher than that of the $Ce_{0.8}Sm_{0.2}O_{1.9}$ (SDC) and 16 mol% yttria-doped zirconia (8YSZ).

The activation energy of the conductivity of $BaCe_{0.8}Y_{0.2-x}Nd_xO_{3-\delta}$, E_a was determined by plotting $\ln(\sigma T)$ vs. $1000/T$ following the Arrhenius equation. Fig. 4 is an Arrhenius plot of the conductivity of $BaCe_{0.8}Y_{0.2-x}Nd_xO_{3-\delta}$ at 600–800 °C, and Table 2 shows the activation energy E_a. Note that the conductivity behavior of $BaCe_{0.8}Y_{0.2-x}Nd_xO_{3-\delta}$ (x = 0–0.1) samples shows an apparently change above 650 °C. An E_a value of 73–83 kJ/mol is calculated in the low temperature range of 500–650 °C. However, an E_a value of 42–60 kJ/mol appears in the high temperature range of 650–800 °C. This indicates that the conductivity mechanism changes as the measured temperature of 650 °C. Dynys reported similar results as this study, but lower in temperature.[14] A probable cause for conductivity mechanism change may be the carrier change from proton to oxygen-ion in high temperatures. There is no apparently conductivity mechanism change in the $BaCe_{0.8}Y_{0.05}Nd_{0.15}O_{3-\delta}$ and $BaCe_{0.8}Nd_{0.2}O_{3-\delta}$ samples above 650 °C, An E_a value of 63–69 kJ/mol was calculated at a temperature range of 500–800 °C. The conductivity of $BaCe_{0.8}Y_{0.2-x}Nd_xO_{3-\delta}$ does not depend on the oxygen vacancy, because the oxygen vacancy concentration does not change as Nd^{3+} replaced Y^{3+}. It was found that the unit volume of $BaCe_{0.8}Y_{0.2-x}Nd_xO_{3-\delta}$ is a little smaller than that of $BaCe_{0.8}Y_{0.2}O_{3-\delta}$ that maybe leads to the decrease of conductivity of $BaCe_{0.8}Y_{0.2-x}Nd_xO_{3-\delta}$ as dopping amount of Nd increases.

Table 2
The activation energy of $BaCe_{0.8}Y_{0.2-x}Nd_xO_{3-\delta}$ in 3 RH% humidity air.

Samples	E_a (500–650 °C), kJ/mol	E_a (650–800 °C), kJ/mol
$BaCe_{0.8}Y_{0.2}O_{3-\delta}$	83	54
$BaCe_{0.8}Y_{0.15}Nd_{0.05}O_{3-\delta}$	74	60
$BaCe_{0.8}Y_{0.1}Nd_{0.1}O_{3-\delta}$	73	42
$BaCe_{0.8}Y_{0.05}Nd_{0.15}O_{3-\delta}$	69	63
$BaCe_{0.8}Nd_{0.2}O_{3-\delta}$	69	68

Fig. 5(a) shows the equivalent circuit for fitting the AC impedance semicircular of $BaCe_{0.8}Y_{0.2-x}Nd_xO_{3-\delta}$ from 600 to 800 °C.[15–17] Z_c is the effect of external wires. R_b and C_g are the grain bulk resistance and capacitance, respectively. R_{gb} and C_{gd} are the grain boundary resistance and capacitance, respectively. R_{ct} is the surface ion diffusion resistance and Z_w is the Warburg impedance. The semicircular arcs in high, medium, and low frequency represent the bulk, grain boundary, and oxygen ion diffusion resistances, respectively.[18] The AC impedance spectra of $BaCe_{0.8}Y_{0.2-x}Nd_xO_{3-\delta}$ samples sintered at 1600 °C in the temperature range 600–800 °C were shown in Fig. 5(b)–(f). The resistance ascribed to the grain resistance at high frequency, grain boundary resistance and oxygen ion diffusion resistance at low frequency. These impedance spectra were analyzed by an equivalent circuit to obtain the resistance and capacitance. Fig. 6 and Table 3 show the bulk (R2), grain boundary (R3), oxygen ion diffusion (R4) and total resistances of $BaCe_{0.8}Y_{0.2-x}Nd_xO_{3-\delta}$ as determined by EIS. The main resistance comes from oxygen ion diffusion, which is larger than the bulk or grain boundary resistances. The bulk, gain boundary, and oxygen ion diffusion resistances apparently decrease as

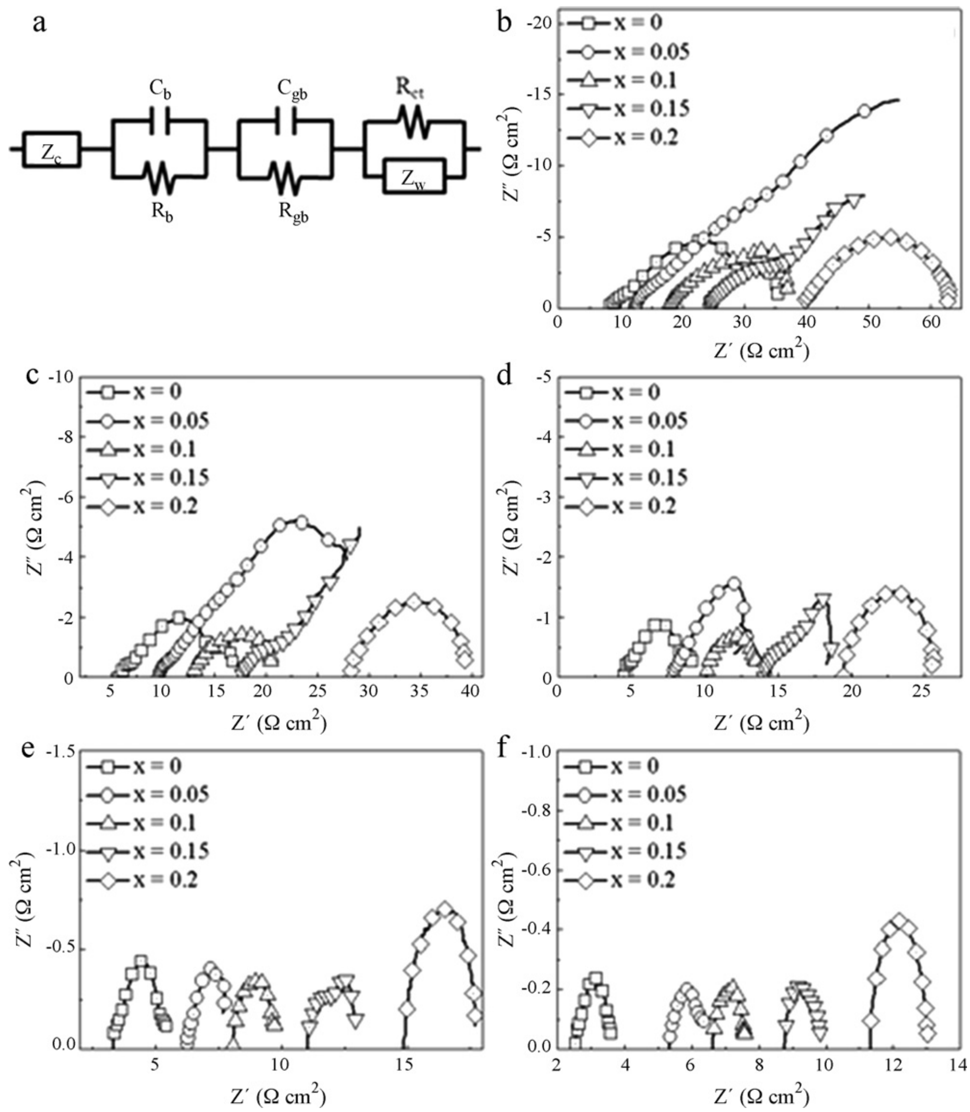

Fig. 5. The equivalent circuit for fitting the AC impedance semicircular and AC impedance spectra of $BaCe_{0.8}Y_{0.2-x}Nd_xO_{3-\delta}$ at (b) 600 °C, (c) 650 °C, (d) 700 °C, (e) 750 °C and (f) 800 °C.

operation temperature increases. The bulk resistance is generally lower than the grain boundary resistance at temperatures ranging from 600 to 700 °C. However, the grain boundary resistance is lower than the bulk resistances at temperatures exceeding 700 °C. The total resistance of $BaCe_{0.8}Y_{0.2-x}Nd_xO_{3-\delta}$ samples increased as the amount of Nd doping increased.

Fig. 7 shows the XRD patterns of $BaCe_{0.8}Y_{0.2-x}Nd_xO_{3-\delta}$ samples in 80 °C water for 24 h. The phase stability of $BaCe_{0.8}Y_{0.2}O_{3-\delta}$ was unstable and second phase of $Ba(OH)_2$ and CeO_2 were detected. The phase stability of $BaCe_{0.8}Y_{0.2-x}Nd_xO_{3-\delta}$ was much better than that of $BaCe_{0.8}Y_{0.2}O_{3-\delta}$, exhibiting no second phase. However, the intensity of $BaCe_{0.8}Y_{0.2-x}Nd_xO_{3-\delta}$ XRD peaks decreased with time even though XRD analysis showed no second phases. This indicates that the phase of $BaCe_{0.8}Y_{0.2-x}Nd_xO_{3-\delta}$ was gradually decomposing. The possible reaction is as follows:

$$BaCeO_3 + H_2O \rightarrow Ba(OH)_2 + CeO_2 \quad (3)$$

The phase decomposition thermal kinetic of all samples was calculated using the Fraction Life Method of Levenspiel.[2] The concentration was calculated from the intensity of XRD peaks. C_A and C_B represent the initial concentration of $BaCe_{0.8}Y_{0.2-x}Nd_xO_{3-\delta}$ and water, respectively. The reaction equation for batch reaction is as follows:

$$-r_A = -\frac{dC_A}{dt} \quad (4)$$

where r_A is rate of the reaction, dC_A is decreased concentration in reaction, and dt is the reaction time.

Eq. (4) is as follows:

$$-r_A = k_1 C_A^a C_B^b \quad (5)$$

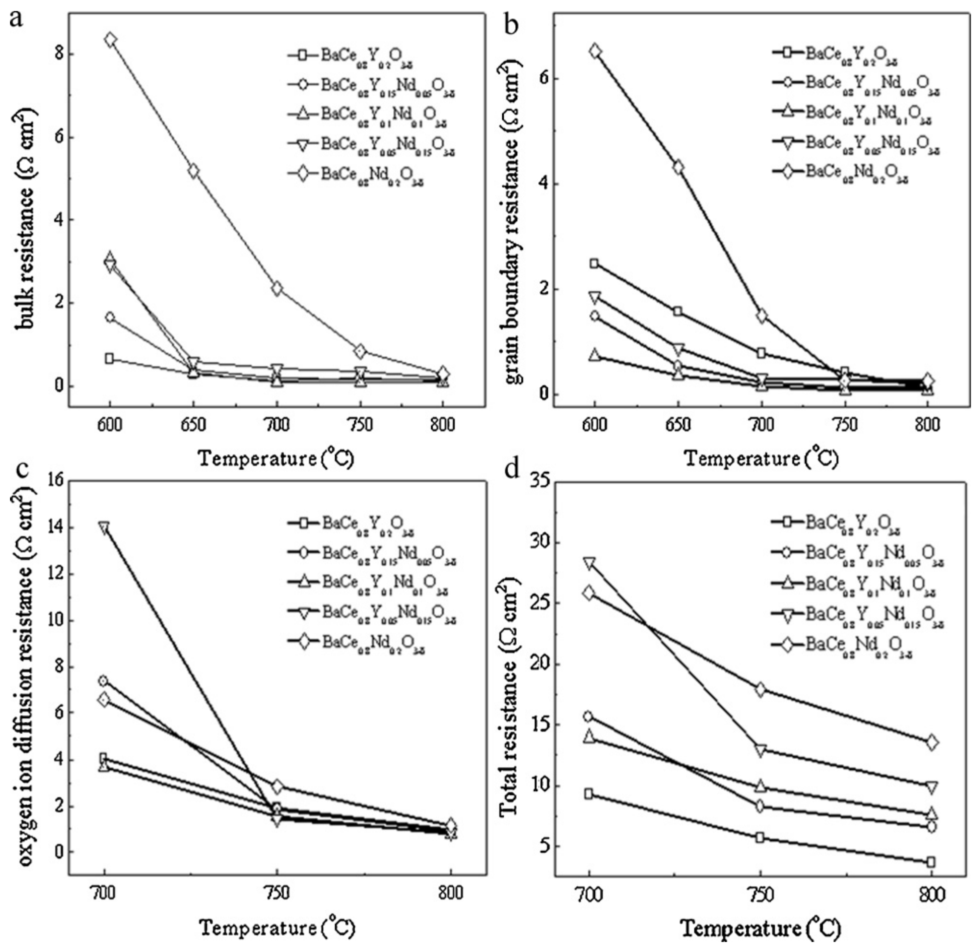

Fig. 6. The (a) bulk resistance, (b) grain boundary resistance, (c) oxygen ion diffusion resistance and (d) total resistance of $BaCe_{0.8}Y_{0.2-x}Nd_xO_{3-\delta}$ at different temperatures.

Table 3
Resistance values of $BaCe_{0.8}Y_{0.2-x}Nd_xO_{3-\delta}$ at different temperatures.

Samples	$\Omega \cdot cm^2$	600 °C	650 °C	700 °C	750 °C	800 °C
$x = 0$	R1	8.46	5.90	4.36	3.14	2.48
	R2	0.66	0.30	0.13	0.22	0.14
	R3	2.48	1.56	0.77	0.41	0.12
	R4	–	–	4.04	1.91	0.94
$x = 0.05$	R1	12.47	9.68	7.87	6.12	5.37
	R2	1.65	0.39	0.21	0.17	0.17
	R3	1.48	0.53	0.23	0.13	0.12
	R4	–	–	7.36	1.87	0.92
$x = 0.1$	R1	17.25	12.81	9.98	8.08	6.64
	R2	3.08	0.33	0.12	0.11	0.11
	R3	0.72	0.35	0.15	0.08	0.06
	R4	–	–	3.69	1.57	0.81
$x = 0.15$	R1	24.38	17.58	13.67	10.92	8.75
	R2	2.93	0.59	0.42	0.37	0.21
	R3	1.88	0.89	0.30	0.28	0.19
	R4	–	–	14.04	1.44	0.84
$x = 0.2$	R1	24.50	18.32	15.47	13.96	11.30
	R2	8.36	5.20	2.36	0.84	0.84
	R3	6.52	4.32	1.49	0.26	0.26
	R4	–	–	6.57	2.84	1.16

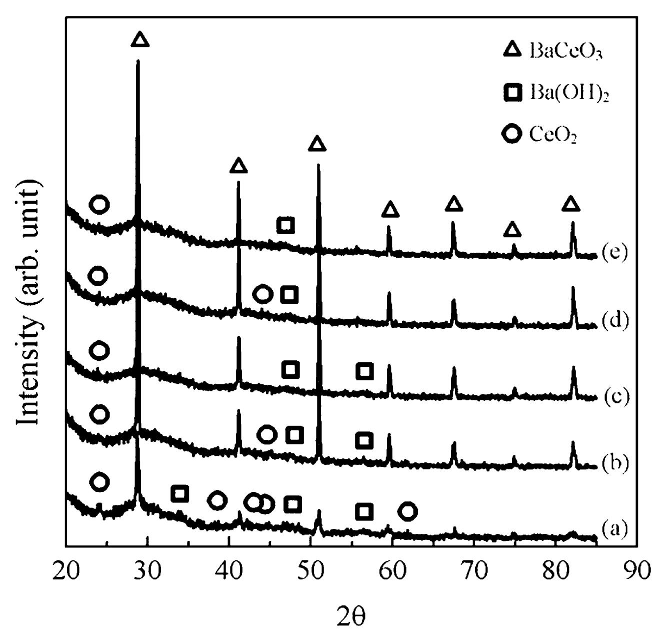

Fig. 7. XRD patterns of (a) $BaCe_{0.8}Y_{0.2}O_{3-\delta}$, (b) $BaCe_{0.8}Y_{0.15}Nd_{0.05}O_{3-\delta}$, (c) $BaCe_{0.8}Y_{0.1}Nd_{0.1}O_{3-\delta}$, (d) $BaCe_{0.8}Y_{0.05}Nd_{0.15}O_{3-\delta}$ and (e) $BaCe_{0.8}Nd_{0.2}O_{3-\delta}$ in 80 °C water for 24 h.

where C_A is the concentration of the sample, C_B is the concentration of water, and k_1 is the reaction constant. The terms a and b represent the reaction order of the sample and water.

$$C_B = \left(\frac{\theta_B}{\theta_A}\right) C_A \tag{6}$$

θ_B/θ_A is the rate of water concentration and the sample concentration. Eq. (7) is a combination of Eq. (5) and Eq. (6):

$$-r_A = k_1 C_A^b \left(\frac{\theta_B}{\theta_A}\right)^b C_A^b \tag{7}$$

$$-r_A = \left[k_1 \left(\frac{\theta_B}{\theta_A}\right)^b\right] C_A^{(a+b)} \tag{8}$$

Eq. (9) replaces $[k_1(\theta_B/\theta_A)^b]$ and $(a+b)$ with the reaction constant k and reaction order n, respectively:

$$-r_A = kC_A^n \tag{9}$$

A combination of Eqs. (4) and (9) was shown in Eq. (10) as follows:

$$-\frac{dC_A}{dt} = kC_A^n \quad n \neq 1 \tag{10}$$

Assuming the concentration decreased 20% with time t_F:

$$C_A^{1-n} - C_{A0}^{1-n} = k(n-1)t; \quad F = 0.8 = \frac{C_A}{C_{A0}} \tag{11}$$

$$t_F = \frac{(0.8)^{1-n} - 1}{k(n-1)} C_{A0}^{1-n} \tag{12}$$

$$\ln\ t_F = \ln \frac{(0.8)^{1-n} - 1}{k(n-1)} + (1-n)\ln\ C_{A0} \tag{13}$$

C_{A0} and t_F were measured from XRD experiment data, Fig. 8 and Table 4 show the reaction order n and reaction constant

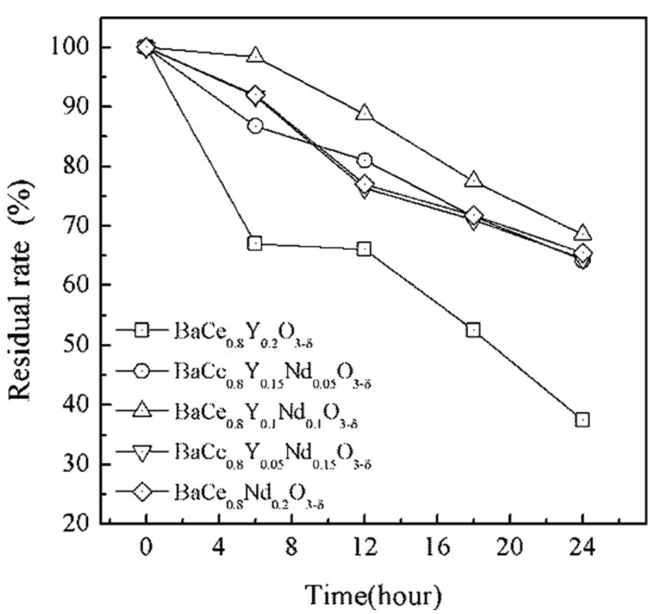

Fig. 8. The residual rate of $BaCe_{0.8}Y_{0.2-x}Nd_xO_{3-\delta}$ dependence on time in 80 °C water.

Table 4
The reaction order n and reaction constant k of $BaCe_{0.8}Y_{0.2-x}Nd_xO_{3-\delta}$ in 80 °C water.

Samples	n	k
$BaCe_{0.8}Y_{0.2}O_{3-\delta}$	1.2743	0.05
$BaCe_{0.8}Y_{0.15}Nd_{0.05}O_{3-\delta}$	1.0345	0.02
$BaCe_{0.8}Y_{0.1}Nd_{0.1}O_{3-\delta}$	1.1646	0.02
$BaCe_{0.8}Y_{0.05}Nd_{0.15}O_{3-\delta}$	1.0715	0.02
$BaCe_{0.8}Nd_{0.2}O_{3-\delta}$	1.1543	0.02

k results. The reaction order n and reaction constant k of $BaCe_{0.8}Y_{0.2-x}Nd_xO_{3-\delta}$ (x = 0.05–0.2) were apparently lower than those of $BaCe_{0.8}Y_{0.2}O_{3-\delta}$. This indicates that doping Nd into the $BaCe_{0.8}Y_{0.2}O_{3-\delta}$ structure improved its phase stability.

4. Conclusions

The structure of $BaCe_{0.8}Y_{0.2-x}Nd_xO_{3-\delta}$ changes to pseudo-orthorhombic structure as Nd doping increases. Results show that $BaCe_{0.8}Y_{0.2}O_{3-\delta}$ exhibited the highest conductivity of 0.028 S/cm at 800 °C in 3 RH% humid air. The conductivities of $BaCe_{0.8}Y_{0.15}Nd_{0.05}O_{3-\delta}$, $BaCe_{0.8}Y_{0.1}Nd_{0.1}O_{3-\delta}$, $BaCe_{0.8}Y_{0.05}Nd_{0.15}O_{3-\delta}$, and $BaCe_{0.8}Nd_{0.2}O_{3-\delta}$ were 0.021 S/cm, 0.015 S/cm, 0.013 S/cm, and 0.01 S/cm, respectively. Electrochemical impedance analysis shows that the resistance is primarily due to oxygen ion diffusion. The bulk resistance is generally lower than the grain boundary resistance at temperatures ranging from 600 to 700 °C. However, the grain boundary resistance is lower than the bulk resistances at temperature exceeding 700 °C. The phase decomposition rate of $BaCe_{0.8}Y_{0.2}O_{3-\delta}$ in 80 °C water is extremely high. The phase stability of $BaCe_{0.8}Y_{0.2-x}Nd_xO_{3-\delta}$ is much better than that of $BaCe_{0.8}Y_{0.2}O_{3-\delta}$. The $BaCe_{0.8}Y_{0.15}Nd_{0.05}O_{3-\delta}$ is a potential SOFC electrolyte due to its high conductivity of 0.021 S/cm and stable structure in water.

Acknowledgements

The authors acknowledge the financial support from the National Science Council in Taiwan under contrast Nos. NSC 100-3113-E-155-001 and NSC 100-3113-E-006-011.

References

1. Minh NQ. Ceramic fuel cells. *J Am Ceram Soc* 1993;**76**:563–88.
2. Fung KZ, Baek HD, Virkar AV. Thermodynamic and kinetic considerations for Bi_2O_3-based electrolytes. *Solid State Ionics* 1992;**52**:199–211.
3. Traina K, Steil MC, Pirard JP, Henrist C, Rulmont A, Cloots R, Vertruyen B. Synthesis of $La_{0.9}Sr_{0.1}Ga_{0.8}Mg_{0.2}O_{2.85}$ by successive freeze-drying and self-ignition of a hydroxypropylmethyl cellulose solution. *J Eur Ceram Soc* 2007;**27**:3469–74.
4. Hari Prasad D, Son JW, Kim BK, Lee HW, Lee JH. Synthesis of nano-crystalline $Ce_{0.9}Gd_{0.1}O_{1.95}$ electrolyte by novel sol–gel thermolysis process for IT-SOFCs. *J Eur Ceram Soc* 2008;**28**:3107–12.
5. Hung IM, Peng HW, Zheng SL, Lin CP, Wu JS. Phase stability and conductivity of $Ba_{1-y}Sr_yCe_{1-x}Y_xO_{3-\delta}$ solid oxide fuel cell electrolyte. *J Power Sources* 2009;**193**:155–9.

6. Iwahara H, Esaka T, Uchida H, Maeda N. Proton conduction in sintered oxides and its application to steam electrolysis for hydrogen production. *Solid State Ionics* 1981;**3**(4):359–63.
7. Ryu KH, Haile SM. Chemical stability and proton conductivity of doped $BaCeO_3$–$BaZrO_3$ solid solutions. *Solid State Ionics* 1999;**125**:355–67.
8. Haile SM, Staneff G, Ryu KH. Non-stoichiometry, grain boundary transport and chemical stability of proton conducting perovskites. *J Mater Sci* 2001;**36**:1149–60.
9. Azad AK, Irvine JTS. Synthesis, chemical stability and proton conductivity of the perovksites $Ba(Ce,Zr)_{1-x}Sc_xO_{3-\delta}$. *Solid State Ionics* 2007;**178**:635–40.
10. Zhong Z. Stability and conductivity study of the $BaCe_{0.9-x}Zr_xY_{0.1}O_{2.95}$ systems. *Solid State Ionics* 2007;**178**:213–20.
11. Virkar AV, Bhide SV. Stability of $BaCeO_3$-based proton conductors in water-containing atmospheres. *J Electrochem Soc* 1999;**146**:2038–44.
12. Yamaguchi S, Yamamoto S, Shishido T, Omori M, Okubo A. Performance of fuel cells based on thin proton conducting oxide electrolyte and hydrogen-permeable metal film anode. *J Power Sources* 2004;**129**:4–6.
13. Levenspiel O. Chemical reaction engineering. In: Anderson W, Hepburn K, Santor K, Murphy K, Perea J, Studios W, Levien B, editors. *Interpretation of batch reactor data*. 3rd ed. New York: John Wiley & Sons, Inc.; 1999. p. 46–9.
14. Dynys FW, Berger MH, Sayir A. Pulsed laser deposition of high temperature protonic films. *Solid State Ionics* 2006;**177**:2333–7.
15. Flint SD, Slade RCT. Variations in ionic conductivity of calcium-doped barium cerate ceramic electrolytes in different atmospheres. *Solid State Ionics* 1997;**97**:457–64.
16. Su XT, Yan QZ, Ma XH, Zhang WF, Ge CC. Effect of co-dopant addition on the properties of yttrium and neodymium doped barium cerate electrolyte. *Solid State Ionics* 2006;**177**:1041–5.
17. Flint SD, Slade RCT. Comparison of calcium-doped barium cerate solid electrolytes prepared by different routes. *Solid State Ionics* 1995;**77**:215–21.
18. Wang JX, Su WH, Xu DP, He TM. Electrical properties of solid solutions $Ba_{1.1}Ce_{1-x}Eu_xO_{3-\delta}$. *J Alloys Compd* 2006;**421**:45–8.